optica

Quantum nonlinear light emission in metamaterials: broadband Purcell enhancement of parametric downconversion: supplementary material

ARTUR DAVOYAN[1,2] AND HARRY ATWATER[1,3]

[1]Resnick Sustainability Institute, Kavli Nanoscience Institute, Department of Applied Physics and Materials Science, California Institute of Technology, 1200 E California Blvd. MC 128-95, Pasadena, California 91125, USA

[2]e-mail: davoyan@caltech.edu

[3]e-mail: haa@caltech.edu

Published 14 May 2018

This document provides supplementary information to "Quantum nonlinear light emission in metamaterials: broadband Purcell enhancement of parametric downconversion," https://doi.org/10.1364/OPTICA.5.000608. Sec. S1 provides key methods used in the Letter. Sec. S2 provides a brief overview of key concepts associated with hyperbolic media. Sec. S3 discusses classical phase matching in quadratically nonlinear hyperbolic media. Sec. S4 discusses the physics of light emission in a generic scenario of a Drude-like metamaterial. Sec. S5 accounts for losses in metamaterials with realistic material parameters. Sec. S6 provides a detailed theoretical derivation. Sec. S7 suggests experimental structures where the predicted phenomena may be observed.

S1. METHODS

Material parameters for silver are taken from experimental data [1]. In our analysis we have assumed that the anisotropy of $LiNbO_3$ is much weaker than that of a host hyperbolic metamaterial. With this assumption we model the permittivity of $LiNbO_3$ as an effective isotropic function being an average between its ordinary and extraordinary permittivity components. The crystal axis of $LiNbO_3$ is considered to be co-aligned with that of hyperbolic metamaterial. For GaP we assumed a 45 degree rotation of GaP crystal axis with respect to that of a hyperbolic metamaterial – this is a standard consideration that ensures maximum nonlinear interaction and wavemixing. The single photon emission rate was estimated assuming a 1 nm spectral filter at the degenerate frequency, i.e., $R = \frac{1}{\hbar\omega}\int\left(\frac{dP}{d\lambda}\right)d\lambda$.

S2. HYPERBOLIC METAMATERIALS AND EFFECTIVE MEDIUM THEORY. BACKGROUND

Progress in nanotechnology, materials science and nanofabrication over recent years has led to design of photonic structures with feature sizes much smaller than the wavelength of the incident light. The electromagnetic properties of such structures may be described by an effective medium approximation, where the optical response is averaged over the light wavelength [2]. It is therefore the cumulative composition of the entire structure, rather than the response of individual structural elements, that determines lightwave propagation in the medium [3]. Importantly, one may design the electromagnetic properties of such effective materials (metamaterials) by controlling the period, element size, and composition of the different materials (e.g., metals with dielectrics) in the structure. With such a design, an electromagnetic response that is typically not attainable in natural materials can be obtained and used for controlling light-matter interaction [2,3].

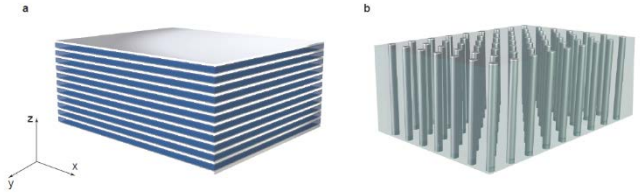

Fig. S1. Schematic illustration of hyperbolic metamaterials. (a) layered hyperbolic media and (b) wire hyperbolic media.

An exciting class of structures is that of so-called hyperbolic metamaterials [4]. Hyperbolic metamaterials are periodic metal-dielectric structures, as schematically shown in Figs. S1(a) and S1(b) (one may find several comprehensive reviews on the subject, see e.g., [4]). As discussed in the main text, these materials behave on average as uniaxial crystals [5] with negative components in their permittivity tensors. Within the frame of the effective medium theory (i.e., when the structure period is much smaller that the wavelength, $\Lambda \ll \lambda$, [2, 3]) the response may be described as:

$$\varepsilon_o = \varepsilon_\perp = \rho\varepsilon_m + (1-\rho)\varepsilon_d \qquad \text{(S2.1)}$$

$$\varepsilon_e = \varepsilon_\parallel = \frac{\varepsilon_m\varepsilon_d}{\rho\varepsilon_d + (1-\rho)\varepsilon_m}$$

in the case of a layered hyperbolic medium, Fig. S1(a), and as

$$\varepsilon_o = \varepsilon_\perp = \frac{(1+\rho)\varepsilon_m\varepsilon_d + (1-\rho)\varepsilon_d^2}{(1+\rho)\varepsilon_d + (1-\rho)\varepsilon_m} \qquad \text{(S2.2)}$$
$$\varepsilon_e = \varepsilon_\parallel = \rho\varepsilon_m + (1-\rho)\varepsilon_d$$

in the case of a wire-like hyperbolic medium, Fig. S1(b). In these expressions ρ denotes metal filling fraction (for instance, for a layer medium $\rho = \frac{h_d}{h_d+h_m}$, where h_d and h_m are dielectric and metal layer thicknesses, respectively).

Light dispersion in hyperbolic structures is then described similarly to regular uniaxial crystals:

$$\frac{k_x^2+k_y^2+k_z^2}{\varepsilon_\perp} = \frac{\omega^2}{c^2} \qquad \text{for ordinary waves} \qquad \text{(S2.3)}$$
$$\frac{k_x^2+k_y^2}{\varepsilon_\parallel} + \frac{k_z^2}{\varepsilon_\perp} = \frac{\omega^2}{c^2} \qquad \text{for extraordinary waves}$$

As was mentioned in the main text, depending on signs of the ordinary and extraordinary permittivities different dispersion regimes may be obtained; see Fig. 2 (a) in the main text.

S3. CLASSICAL PHASE MATCHING ANALYSIS

In a classical nonlinear system, the efficiency of nonlinear interaction and wavemixing critically depends on phase matching between the propagating waves. In this section, we derive and analyze phase matching conditions for a nonlinear hyperbolic metamaterial based on the dispersion relations for ordinary and extraordinary waves, Eqs. (S2.3). For simplicity, we consider degenerate wavemixing, i.e., $\omega_s = \omega_i = \frac{\omega_p}{2}$. We also assume two specific scenarios of pump propagation: along the crystal axis (i.e., $\boldsymbol{k}_p \parallel \boldsymbol{z}$) and perpendicular to it (i.e., $\boldsymbol{k}_p \parallel \boldsymbol{x}$). Finally, we limit our analysis to the case of downconversion into extraordinary signal and extraordinary idler waves (other cases, such as conversion into ordinary-ordinary and extraordinary-ordinary waves, are quite similar to those of crystals with a regular material dispersion).

Pump propagation along the crystal axis $\boldsymbol{k}_p \parallel \boldsymbol{z}$. Assuming that n_p is the effective index of the pump wave in the direction of propagation, we can express the pump wavevector as $k_{pz} = \frac{\omega_p}{c} n_p$, n_p is the refractive index at pump frequency. It is convenient to represent the signal and idler wavevectors as $\boldsymbol{k} = \boldsymbol{k}_\perp + \boldsymbol{k}_\parallel$, where $\boldsymbol{k}_\parallel$ is the component of the wavevector parallel to the direction of pump propagation (in this particular case it is the z component) and $\boldsymbol{k}_\perp$ is the component of the wavector that is perpendicular to the pump (the notation not to be mixed with $\varepsilon_\parallel$ and $\varepsilon_\perp$ which are defined with respect to the crystal symmetry axis). Phase matching in a degenerate case, $\omega_s = \frac{\omega_p}{2}$, would require that $2k_{sz} = k_{pz}$, $k_{sz} = k_{iz}$ and $\boldsymbol{k}_{s\perp} = -\boldsymbol{k}_{i\perp}$. Substituting these conditions into the dispersion equations for signal and idler waves, we get:

$$\frac{k_{s\perp}^2}{\varepsilon_{s\parallel}} + \frac{k_p^2}{4\varepsilon_{s\perp}} = \frac{\omega_p^2}{4c^2} = \frac{k_p^2}{4n_p^2} \qquad \text{(S3.1)}$$

After a little bit of algebra it is possible to show that:

$$k_{s\perp}^2 = \frac{\omega_s^2}{c^2}\left(\varepsilon_{s\parallel} - n_p^2\frac{\varepsilon_{s\parallel}}{\varepsilon_{s\perp}}\right) \qquad \text{(S3.2)}$$

here $\varepsilon_{s\perp}$ and $\varepsilon_{s\parallel}$ are components of the permittivity tensor at the signal photon frequency.

Exact phase matching in a lossless structure is possible when the transverse signal (idler) wavevectors are real, implying that $k_{s\perp}^2 > 0$. For $\varepsilon_{s\parallel} > 0$ and $\varepsilon_{s\perp} > 0$, i.e., in regular crystals, phase matching is possible only when $n_p^2 < \varepsilon_{s\perp}$. This condition is hard to achieve in crystals with normal material dispersion, in which the refractive index monotonically grows with frequency. This effect is especially pronounced in high refractive index structures and semiconductors near the band-gap edge (e.g., gallium phosphide discussed in the main text), challenging their use in nonlinear applications.

In the regime $\varepsilon_{s\perp} < 0$ and $\varepsilon_{s\parallel} > 0$, which is typically attained in a layered hyperbolic media [Fig. S1(a)] phase matching is automatically satisfied. In particular, for any $n_p^2 > 0$ (i.e., for any propagating pump in the crystal) there always exists a pair of signal–idler waves.

Finally, in a wire hyperbolic medium ($\varepsilon_{s\perp} > 0$ and $\varepsilon_{s\parallel} < 0$) phase matching is possible for $n_p^2 > \varepsilon_{s\perp}$, see also Fig. 3(b) in the main text. We note that for $n_p^2 < \varepsilon_{s\perp}$ exact phase matching is satisfied for ordinary waves.

The locus of points in the $\boldsymbol{k}$ space for which phase matching is achieved determines directions of nonlinear light emission, i.e., the angular distribution of the emission pattern. Clearly, for a pump propagating along the $\boldsymbol{z}$ axis, which is the high symmetry axis of the crystal, the emission patterns for all the studied cases are radially symmetric, i.e., $\boldsymbol{k}_{s\perp} = const$, see Figs. 3(a) and 3(b) in the main text.

Pump propagation along the x axis, $\boldsymbol{k}_p \parallel \boldsymbol{x}$. For this direction of pump propagation the phase matching condition requires that $2k_{sx} = k_{px}$. Substituting this condition into the dispersion equation for the extraordinary waves [Eqs. (S2.3)] we arrive at the following expression:

$$k_{sy}^2 + k_{sz}^2\frac{\varepsilon_{s\parallel}}{\varepsilon_{s\perp}} = \frac{\omega_s^2}{c^2}\left(\varepsilon_{s\parallel} - n_p^2\right) \qquad \text{(S3.3)}$$

Phase matching is possible when propagating signal (idler) solutions exist, i.e., $k_{sy}^2 > 0$ and $k_{sz}^2 > 0$. For a regular crystal ($\varepsilon_{s\parallel}\varepsilon_{s\perp} > 0$), this condition is satisfied only for $n_p^2 < \varepsilon_{s\parallel}$, which is again hard to obtain in materials with normal dispersion. The emission pattern in this case is elliptical, $k_{sy}^2 + k_{sz}^2\frac{\varepsilon_{s\parallel}}{\varepsilon_{s\perp}} = const$.

In the hyperbolic regime, when $\varepsilon_{s\perp}\varepsilon_{s\parallel} < 0$, we find that the phase matching condition is always satisfied. That is, one can always find k_{sy} and k_{sz} that satisfy Eq. (S3.3). Interestingly, in this scenario light emission is hyperbolic (see. Figs. 3(c) and 3(d) in the main text). Furthermore, for a layered hyperbolic medium ($\varepsilon_{s\perp} < 0$ and $\varepsilon_{s\parallel} > 0$) there is a transition point at $n_p^2 = \varepsilon_{s\parallel}$, at which the emission goes from a single hyperbolic to a double hyperbolic shape (this is easy to see from the geometry of the isofrequency surface, as shown in Fig. S2(f)).

S4. PRINCIPLES OF HYPERBOLIC EMISSION

In the main text we showed that in the hyperbolic regime of operation signal photon emission rate may be substantially enhanced as compared to the case of a bulk crystal. In particular, we have calculated signal photon spectral power density, which we found to be expressed as:

$$\frac{dP_s}{d\lambda_s} = \frac{\hbar\pi c^3 L^2}{\lambda_s^4\lambda_i}\frac{P_p}{\varepsilon_0 n_p}\int d^2\boldsymbol{k}_{s\perp}\frac{\partial k_{s\parallel}}{\partial\omega}\frac{\partial k_{i\parallel}}{\partial\omega}\, c_{\boldsymbol{k}_s}^2 c_{\boldsymbol{k}_i}^2 \times$$
$$N(\boldsymbol{k}_s,\boldsymbol{k}_i)\left|\frac{1-e^{i\Delta k_\parallel L}}{i\Delta\boldsymbol{k}_\parallel L}\right|^2 e^{-i\gamma'(\boldsymbol{k}_s)L} \qquad \text{(S4.1)}$$

where $N(\boldsymbol{k}_s,\boldsymbol{k}_i) = \left|\sum_{lmn}\bar{\bar{\chi}}_{lmn}^{(2)}u_l(\omega_p)u_m(\omega_s)u_n(\omega_i)\right|^2$.

This expression is rather complex to analyze directly. On the other hand, in the theory of nonlinear optics of crystals it is frequently assumed that the nonlinear wave interaction and mixing may be described by some effective nonlinearity, which mathematically implies that $N(\boldsymbol{k}_s,\boldsymbol{k}_i) \to const$. In this limit the integral simplifies to:

$$G(\omega_s,\omega_p) = \int d^2\boldsymbol{k}_{s\perp}\, c_{\boldsymbol{k}_s}^2 c_{\boldsymbol{k}_i}^2\frac{\partial k_{s\parallel}}{\partial\omega}\frac{\partial k_{i\parallel}}{\partial\omega}\left|\frac{1-e^{i\Delta k_\parallel L}}{i\Delta\boldsymbol{k}_\parallel L}\right|^2 e^{-i\gamma'(\boldsymbol{k}_s)L} \qquad \text{(S4.2)}$$

and depends on signal and idler wave dispersions (embedded into coefficients $c_{\boldsymbol{k}_s}^2 c_{\boldsymbol{k}_i}^2$), the group velocities in the direction of pump propagation ($\frac{\partial k_{s\parallel}}{\partial\omega}$ and $\frac{\partial k_{i\parallel}}{\partial\omega}$), phase matching ($\left|\frac{1-e^{i\Delta k_\parallel L}}{i\Delta\boldsymbol{k}_\parallel L}\right|^2$), and the signal photon dissipation ($e^{-i\gamma'(\boldsymbol{k}_s)L}$).

In this section, we explore the dynamics of this integral in the hyperbolic regime. In contrast to the main text and section S5, where we use experimental material parameters (see also sections S1 and S5), here, for the sake of simplicity of our analysis, and without loss of generality, we consider hyperbolic structures comprised of a nondispersive dielectric with a permittivity $\varepsilon_d = 2$ and a Drude metal with $\varepsilon_m = 1 -$

$\frac{\omega_{plasm}^2}{\omega(\omega-ig)}$, where ω_{plasm} is the plasma frequency and g is the collision frequency; the metal filling fraction is assumed to be 30% (i.e., $\rho = 0.3$). It is convenient to introduce a wavelength λ_{ENZ} for which $\rho\varepsilon_m + (1-\rho)\varepsilon_d = 0$, i.e., at which either ordinary component (for layer-hyperbolic) or extraordinary component (for wire-hyperbolic) of the permittivity tensor go through the epsilon-near-zero point (ENZ) (see Eqs. (S2.1) and (S2.2)).

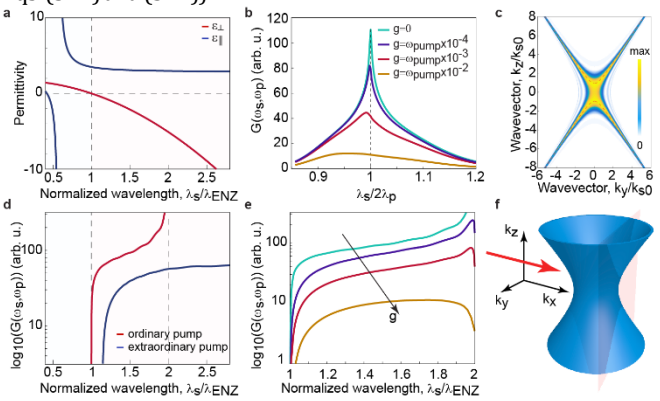

Fig. S2. Spontaneous parametric downconversion in Drude layered hyperbolic medium. (a) dispersion of the ordinary and extraordinary permittivities of a Drude layered hyperbolic medium. (b) spectral variation of the function $G(\omega_s, \omega_p)$ for several different values of the collision frequency, g. Here $\lambda_p = \lambda_{ENZ}/1.2$. (c) k-space distribution of the expression under the integral (S4.2) showing the angular variation of the single photon probability. Here it is assumed that $g = 10^{-3}\omega_{plasma}$ and $\lambda_p = \lambda_{ENZ}/0.9$. Dashed lines denote the emission patterns estimated from simple phase matching analysis. (d) logarithmic scale variation of the function $G(\omega_s, \omega_p)$ in a degenerate regime ($\lambda_s = 2\lambda_p$) for two different pump polarizations in a lossless case ($g = 0$). (e) logarithmic scale variation of the function $G(\omega_s, \omega_p)$ in a degenerate regime for ordinary pump polarization for values of the collision frequency, g, as in panel (b). In panels (b-e) propagation length is assumed to be $L = 3\lambda_{ENZ}$. (f) schematic illustration of the extraordinary wave isofrequency contour for a layered hyperbolic medium. The arrow denotes the direction of the pump propagation. The cross-section plane schematically explains the origin of the emission pattern observed in panel (c).

Figures S2(a) and S3(a) show dispersion plots for effective ordinary and extraordinary components of the permittivity tensor for layer and wire hyperbolic media, respectively. For wavelengths longer than λ_{ENZ} in both of these cases, the system is in the hyperbolic dispersion regime (i.e., $\varepsilon_\parallel\varepsilon_\perp < 0$). As was discussed in the main text, we consider pumping in the elliptical and emission in the hyperbolic parts of the spectrum (Fig. 2(b) in the main text). A pump wave propagating in the $\boldsymbol{x}$ direction (perpendicular to the crystal axis) can have two possible polarization states: ordinary ($k_{pz} = \frac{\omega}{c}n_p$, with $n_p = \sqrt{\varepsilon_\perp}$) and extraordinary ($k_{pz} = \frac{\omega}{c}n_p$, with $n_p = \sqrt{\varepsilon_\parallel}$). The choice of pump polarization would influence the phase matching conditions.

Typical spectra of the function $G(\omega_s, \omega_p)$ for a layered hyperbolic medium are shown in Fig. S2(b) (here an ordinary pump wave is assumed, $L = 3\lambda_{ENZ}$, and $\lambda_p = \lambda_{ENZ}/1.2$). For the lossless case, the emission is peaked exactly at the degenerate wavelength $\lambda_s = \lambda_p/2$. With increasing losses to the system (i.e., increase of g), the emission peak shifts to shorter wavelengths. We attribute this break of symmetry to the frequency dispersion of losses in the system (losses are more pronounced closer to the ENZ point). A similar trend is also seen in the Fig. 4(b) in the main text.

In Fig. S2(d) we plot the function $G(\omega_s, \omega_p)$ at the degenerate wavelength ($\lambda_s = 2\lambda_p$) in the lossless limit. At the edge of the elliptical-to-hyperbolic transition function $G(\omega_s, \omega_p)$ vanishes (we note that at this wavelength range, close to the near-zero-epsilon point, our perturbative approach might not be fully sufficient). With increasing pump wavelength, i.e., with getting deeper into the hyperbolic domain for signal waves, the function $G(\omega_s, \omega_p)$ dramatically increases, manifesting a dramatic increase in the light emission in the hyperbolic regime. Such an enhancement is associated with phase mismatch free operation and a dramatic growth of the available signal wave phase volume (we again assume here that the maximum wavevector is bound, $k_{zmax} = 10\frac{2\pi}{\lambda_{ENZ}}$, so that the phase volume is always finite). Finally, for the ordinary pump, as $n_p = \sqrt{\varepsilon_\perp} \to 0$, $G(\omega_s, \omega_p)$ diverges. This divergence is essentially a mathematical artifact attributed to the lossless ENZ medium (to sustain a finite pump power in the system an infinitely high electric field is required; this is unphysical). However, in a realistic system the growth of $G(\omega_s, \omega_p)$ is limited by losses in the system, as is clearly shown in Fig. S2(e). Importantly, the function $G(\omega_s, \omega_p)$ is enhanced over a broad range of pump (signal) wavelengths in the hyperbolic regime. Similar dynamics is observed in the case of structures with realistic material parameters (see Fig. 4 in the main text). In particular, we see an initial growth of the peak emission right after the ENZ point for signal waves followed by a broad range of enhanced light emission, and, finally, by a subsequent decrease in the light emission close to the ENZ point for the pump wave (see Figs. 4(a) and 4(b) in the main text).

Next, we analyze the angular distribution of light emission in such an idealistic Drude layered hyperbolic medium. The corresponding emission pattern is shown in the Fig. S2(c). The shape of the emission pattern is hyperbolic and coincides with our simple phase matching analysis. Fringes in the pattern are characteristic of the $\mathrm{sinc}(\Delta\boldsymbol{k}L)$ at small propagation distances. As $L \to \infty$ the emission pattern collapses to a curve $\Delta\boldsymbol{k} = 0$. We find that the maximum emission occurs for smaller signal (idler) wavevectors, $\boldsymbol{k}$, and rapidly decreases with the $\boldsymbol{k}$ increase. This behavior is associated with a stronger damping for higher $\boldsymbol{k}$ modes, as expected. Strong emission for $|\boldsymbol{k}_\perp|/|\boldsymbol{k}_{s0}| < 3$ suggests that the emitted signal light may be efficiently collected by adjacent high index dielectric media. A similar hyperbolic emission pattern is shown for the case of a silver – gallium phosphide layered hyperbolic medium (Fig. 4(f) in the main text). However in that case, the influence of the $N(\boldsymbol{k}_s, \boldsymbol{k}_i)$ term under the integral (i.e., mixing of light polarizations) modifies the emission pattern.

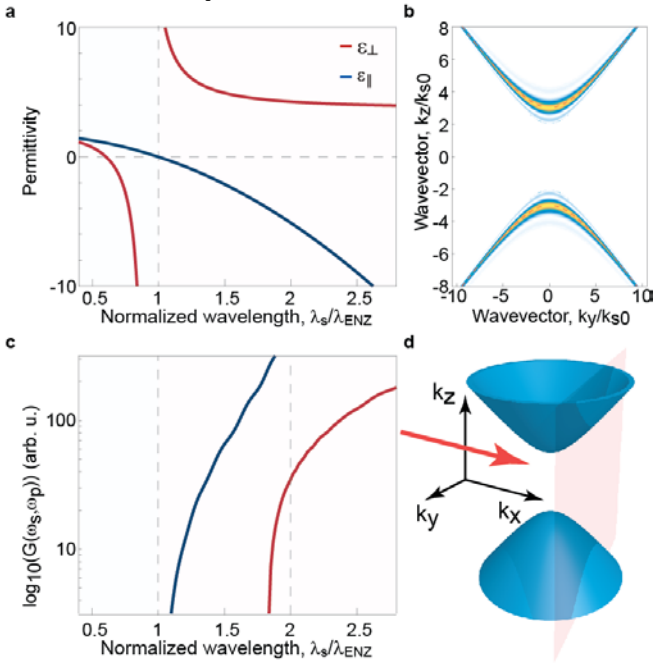

Fig. S3. Spontaneous parametric downconversion in a wire hyperbolic medium. (a) dispersion of the ordinary and extraordinary permittivities of a Drude layered hyperbolic medium. (b) k-space distribution of the expression under the integral (S4.2) showing the angular variation of

the single photon probability. Here it is assumed that $g = 10^{-3}\omega_{plasma}$ and $\lambda_p = \lambda_{ENZ}/0.9$. Dashed lines denote the emission patterns estimated from the simple phase mateching analysis. (c) logarithmic scale variation of the function $G(\omega_s, \omega_p)$ in a degenerate regime ($\lambda_s = 2\lambda_p$) for two different pump polarizations in a lossless case ($g = 0$). (d) schematic illustration of the extraordinary wave isofrequency contour for a wire hyperbolic medium. The arrow denotes the direction of the pump propagation. The cross-section plane schematically explains the origin of the emission pattern observed in panel (b).

The case of a hyperbolic wire-like medium is studied in Fig. S3. Similar to the layer-medium case, the emission (function $G(\omega_s, \omega_p)$) grows dramatically with increasing pump wavelength (i.e., as signal wavelength is pushed deeper into the hyperbolic wavelength range), Fig. S3(c). The emission pattern is double hyperbolic [Fig. S3(b)], as expected from the phase matching analysis, see Figs. 3(c) and 3(d) in the main text. Similarly to the layered-hyperbolic medium, higher k-wavevectors are strongly attenuated.

S5. HYPERBOLC Ag-LiNbO3 AND Ag-GaP STRUCTURES

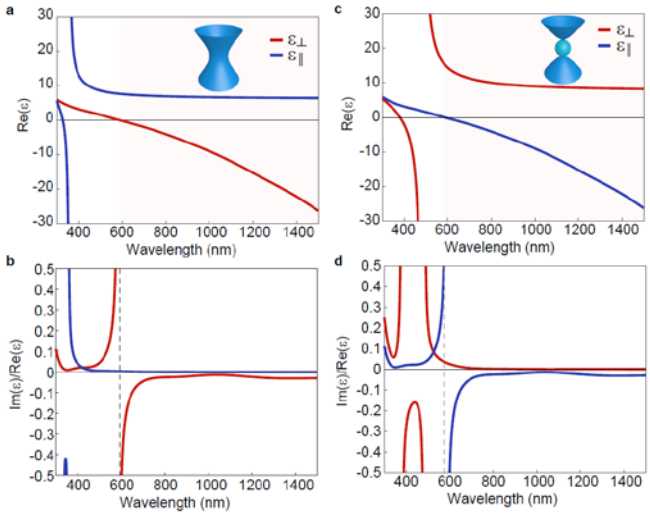

Fig. S4. Effective medium parameters for $LiNbO_3$ – Ag hyperbolic media with 80 nm period and 25% metal filling fraction. (a) dispersion of the real part of the ordinary and extraordinary components of the effective permittivity tensor for a layer-hyperbolic medium. Inset shows the isofrequency surface. (b) Dispersion of the material "quality factor" defined as the ratio of the imaginary to real part of the permittivity. (c) and (d) are the same as (a) and (b) but for a wire-hyperbolic metamaterial.

We next analyze the effective material parameter dispersion for the structures studied in the main text. In Figs. S4(a) and S4(b), we plot the dispersion of ordinary ($\varepsilon_\perp$) and extraordinary ($\varepsilon_\parallel$) components of the effective permittivity tensor, Eq. (S2.1) and Eq. (S2.2), for layer-hyperbolic, Fig. S4(a), and wire-hyperbolic, Fig. S4(b), silver – lithium niobate structures. We consider here a structure with 80nm period and a 25% metal filling fraction; we also take into account actual experimental and material parameters (for $LiNbO_3$ we used Ref. [6] and for GaP Ref. [7]). For both of the structures depicted, there is an epsilon-near-zero point around λ=600 nm, i.e., for longer wavelengths the system is in the hyperbolic dispersion band, whereas for shorter wavelengths it exhibits elliptical dispersion. The fact that λ_{ENZ} is much larger than the period structure (which here is 80 nm) justifies the use of the effective medium theory. Note that the epsilon-near-zero point may be tuned by appropriate choice of the structure period and filling fraction.

In order to estimate the influence of losses in the structure, we plot $\mathrm{Im}(\varepsilon_\perp)/\mathrm{Re}(\varepsilon_\perp)$ and $\mathrm{Im}(\varepsilon_\parallel)/\mathrm{Re}(\varepsilon_\parallel)$ for both layer-hyperbolic, Fig. S4(c), and wire-like hyperbolic, Figs. S4(d), structures. These functions physically correspond to the 'quality factor' of the medium. We find that away from the epsilon-near-zero points $\left|\frac{\mathrm{Im}(\varepsilon)}{\mathrm{Re}(\varepsilon)}\right| < 0.1$ implying that within the hyperbolic regime of interest the wave attenuation is not as strong. For instance, for the $\boldsymbol{x}$ direction propagation of ordinary waves, we get $k_x = k_x' + ik_x'' = \frac{\omega}{c}\sqrt{\varepsilon_\perp} \simeq \frac{\omega}{c}\sqrt{\mathrm{Re}(\varepsilon_\perp)} + i\frac{\omega}{2c}\sqrt{\mathrm{Re}(\varepsilon_\perp)}\frac{\mathrm{Im}(\varepsilon_\perp)}{\mathrm{Re}(\varepsilon_\perp)}$. The propagation length in terms of light wavelength in the medium is then simply $\mathcal{L} = \frac{k_x'}{2k_x''} = \frac{\mathrm{Re}(\varepsilon_\perp)}{\mathrm{Im}(\varepsilon_\perp)}$, which is according to Figs. S4(c) and S4(d) is over 30 wavelengths for a layer-hyperbolic and over 100 wavelengths for a wire-hyperbolic media. Similar estimates may be carried out for extraordinary waves. We note that the use of relative propagation length $\mathcal{L}$ is justified, despite the seemingly short absolute propagation length, because the short mode wavelength reduces the absolute interaction length. Relative propagation length, therefore, gives a good estimate of the absorption in the system.

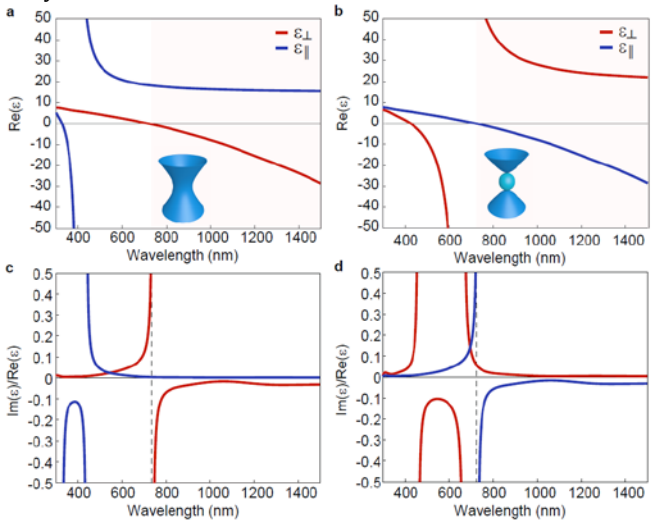

Fig. S5. Effective medium parameters of GaP – Ag hyperbolic media with a 100 nm period and 30% metal fill fraction. (a) dispersion of ordinary and extraordinary components of the effective permittivity tensor for a layer-hyperbolic medium. Inset shows the isofrequency surface. (b) Dispersion of the material "quality factor" defined as the ratio of the imaginary to real part of the permittivity. (c) and (d) are the same as (a) and (b) but for a wire-hyperbolic metamaterial.

We apply a similar analysis to study the case of gallium phosphide-based hyperbolic media, see Fig. S5. Here we assume that the period of the structure is 100 nm and the metal filling fraction is 30%. The elliptical-to-hyperbolic transition is at around λ=750 nm, see Figs. S5(a) and S5(b). Finally, since GaP is practically lossless above 450 nm, in the hyperbolic regime we obtain material-dependent quality factors similar to those of Ag-$LiNbO_3$ structures, Figs. S5(c) and S5(d).

S6. SPONTANEOUS PARAMETRIC DOWNCONVERSION EMISSION RATE AND POWER

In this section, we develop a quantum theory that allows us to estimate the probability of signal photon generation through spontaneous parametric downconversion (SPDC) in uniaxial crystals with quadratic nonlinearity, and dispersive and lossy effective permittivity tensor $\bar{\bar{\varepsilon}} = \mathrm{diag}(\varepsilon_\perp, \varepsilon_\perp, \varepsilon_\parallel)$. We develop a theory that may be capable of describing SPDC in either of the scenarios shown in Fig. 1(c) of the main text: regular elliptical (with loss and dispersion), layer-hyperbolic and wire-hyperbolic cases.

In principle, there are two approaches in developing such a theory: microscopic and macroscopic [8-16]. In a microscopic picture one considers both electromagnetic field and matter degrees of freedom

and, thus, accounting explicitly for light-matter interaction, dissipation, and dispersion [11-13]. However, such a formulation in case of an extreme anisotropy and material nonlinearity becomes rather cumbersome, and hard to analyze and implement. The macroscopic picture is a standard formalism for quantum optics of dielectric media [10,15]. Within the scope of this theory a classical macroscopic electromagnetic field is quantized. Previously, macroscopic theory was utilized to describe spontaneous parametric downconvesion in a quasi-isotropic, lossless, and dispersionless limit [16-18]. Ref. [26] proposed a Green's function formalism for accounting for spontaneous nonlinear wavemixing in complex systems. Here we develop a conceptually different framework for accounting for spontaneous parametric downconversion in the general case of lossy and dispersive medium with arbitrary anisotropy which is more intuitive and straightforward, and may provide deeper insight into the physics of quantum nonlinear processes. Specifically, we base our analysis on a macroscopic picture, considering eigenmode configuration and take into account material losses and dispersion perturbatively.

We consider that the electric field in the crystal may be presented as a sum of interacting pump, signal and idler waves: $\boldsymbol{E} = \boldsymbol{E}_p + \boldsymbol{E}_s + \boldsymbol{E}_i$. We treat the pump classically and explore the quantum mechanical spontaneous generation of signal and idler photons. For this reason, we write down the Hamiltonian of the system:

$$\hat{\mathcal{H}} = \hat{\mathcal{H}}_{lin} + \hat{\mathcal{H}}_{int} \tag{S6.1}$$

where $\hat{\mathcal{H}}_{lin}$ is the linear part of the Hamiltonian corresponding to the self-energy of the interacting fields, and $\hat{\mathcal{H}}_{int}$ is the energy of the system associated with the nonlinear interaction between signal, idler and pump waves.

The self-energy associated with either of the interacting fields to the first order approximation of dispersion theory may be expressed as [17,19]:

$$\hat{\mathcal{H}}_{lin}^{s,i} = \frac{1}{2}\int_V d^3\boldsymbol{r}\left[\frac{1}{\mu_0}\hat{\boldsymbol{B}}^2 + \varepsilon_0\hat{\boldsymbol{E}}\bar{\bar{\varepsilon}}\hat{\boldsymbol{E}} + \varepsilon_0\omega\hat{\boldsymbol{E}}\frac{\partial\bar{\bar{\varepsilon}}}{\partial\omega}\hat{\boldsymbol{E}}\right]_{s,i} \tag{S6.2}$$

here the field operators $\hat{\boldsymbol{B}}$ and $\hat{\boldsymbol{E}}$, and material parameters are to be taken at corresponding signal and idler wave frequencies. The integration is over the quantization volume of the crystal $V = A \times L$, where A is the crystal area perpendicular to the pump propagation direction and L is the distance along the propagation direction (i.e., interaction length).

The interaction Hamiltonian, in turn, is given by the following expression [20-22]:

$$\hat{\mathcal{H}}_{int} = \varepsilon_0\int_V d^3\boldsymbol{r}\sum_{lmn}\bar{\bar{\chi}}^{(2)}_{lmn}E_l(\omega_p)E^+_m(\omega_s)E^+_n(\omega_i) + H.c. \tag{S6.3}$$

where $\bar{\bar{\chi}}^{(2)}$ is the second order nonlinear susceptibility tensor of the crystal, which is assumed to be nondispersive and possessing Klienman's symmetry [22].

We use a standard approach to field quantization, in which the interacting signal and idler fields are decomposed into plane eigen-modes of the crystal [8]. In this case the electric field operator is given as:

$$\hat{\boldsymbol{E}}_\xi = \frac{1}{\sqrt{V}}\sqrt{\frac{\hbar\omega_\xi}{\varepsilon_0}}\sum_\nu\sum_{\boldsymbol{k}_{\xi\nu}} c_{\boldsymbol{k}_{\xi\nu}}\boldsymbol{u}_{\boldsymbol{k}_{\xi\nu}}\hat{a}_{\boldsymbol{k}_{\xi\nu}}e^{i\boldsymbol{k}_{\xi\nu}r - i\omega_\xi t} + H.c. \tag{S6.4}$$

where $\hat{a}_{\boldsymbol{k}_{\xi\nu}}$ and $\hat{a}^+_{\boldsymbol{k}_{\xi\nu}}$ are photon annihilation and creation operators, respectively, index $\xi = \{s, i\}$ differentiates signal and idler waves, index ν runs over ordinary and extraordinary waves that may exist in the uniaxial crystal. The electric field polarizations $\boldsymbol{u}_{\boldsymbol{k}_{\xi\nu}}$ of the crystal in a general case are given as eigenmode solutions of the Fresnel equation [5]:

$$\boldsymbol{u} = \begin{bmatrix} u_x \\ u_y \\ u_z \end{bmatrix} = u_0\begin{bmatrix} \dfrac{k_x}{k^2 - \dfrac{\omega^2}{c^2}\varepsilon_\perp} \\ \dfrac{k_y}{k^2 - \dfrac{\omega^2}{c^2}\varepsilon_\perp} \\ \dfrac{k_z}{k^2 - \dfrac{\omega^2}{c^2}\varepsilon_\parallel} \end{bmatrix} \tag{S6.5}$$

where we dropped indexes for simplicity. The normalization is chosen such that polarizations satisfy orthonormality condition $\boldsymbol{u}_{\boldsymbol{k}_{\xi\nu}}\boldsymbol{u}'_{\boldsymbol{k}_{\xi\nu}} = \delta_{\nu\nu'}$. A special treatment is needed when $k^2 = \frac{\omega^2}{c^2}\varepsilon_{\perp,\parallel}$. Thus for the case of ordinary waves $k^2 = \frac{\omega^2}{c^2}\varepsilon_\perp$ polarization reduces to $\boldsymbol{u} = u_0(k_y, -k_x, 0)$, whereas for extraordinary waves, when $k^2 = \frac{\omega^2}{c^2}\varepsilon_\parallel$ polarization is given simply as $\boldsymbol{u} = (0,0,1)$. The wavevectors $\boldsymbol{k}_{\xi\nu}$ for a given frequency ω_ξ may be found from the respective dispersion equations for ordinary and extraordinary waves, see Eq. (S2.3). Lastly, in Eq. (S6.4) normalization coefficients $c_{\boldsymbol{k}_{\xi\nu}}$ are chosen such that the energy of each of the eigen-modes $\boldsymbol{k}_{\xi\nu}$ is quantized in the units of $\hbar\omega_\xi$:

$$c_{\boldsymbol{k}_{\xi\nu}} = \left[\boldsymbol{u}_{\boldsymbol{k}_{\xi\nu}}\bar{\bar{\varepsilon}}_\xi\boldsymbol{u}_{\boldsymbol{k}_{\xi\nu}} + \frac{1}{2}\boldsymbol{u}_{\boldsymbol{k}_{\xi\nu}}\omega_\xi\frac{\partial\bar{\bar{\varepsilon}}_\xi}{\partial\omega}\boldsymbol{u}_{\boldsymbol{k}_{\xi\nu}}\right]^{-1/2} \tag{S6.6}$$

The pump field is considered to be classical and is expressed as:

$$\boldsymbol{E}_p = \frac{1}{2}\sqrt{\frac{2P_p}{\varepsilon_0 c n_p A}}\boldsymbol{u}_p e^{i\boldsymbol{k}_p\boldsymbol{r} - i\omega t} + c.c. \tag{S6.7}$$

where n_p is the effective index of the pump wave along the direction of pump propagation, P_p is the pump power in the crystal.

Next, we use Fermi's Golden rule to estimate the single photon generation rate. We assume that the losses are weak and do not perturb the nonlinear interaction and spontaneous photon downconversion. Specifically, we consider that the probabilities of photon emission and subsequent photon absorption are independent of each other. In this case the rate of generation of signal photons with a given frequency ω_s and wavevector $\boldsymbol{k}_s(\omega_s)$ for all possible idler waves can be written as [17,23]:

$$\mathcal{R}_s(\omega_s, \boldsymbol{k}_s) = \frac{2\pi}{\hbar}\times$$
$$\int_{\mathcal{V}_i}\frac{V}{8\pi^3\hbar}\left|< f\left|\hat{\mathcal{H}}_{int}\right|0>\right|^2\delta(\omega_p - \omega_s - \omega_i)d^3\boldsymbol{k}_i \tag{S6.8}$$

here, as was mentioned in the main text, $|0>$ corresponds to a state containing no signal and idler photons, and $< f|$ is the final state with one signal photon with frequency ω_s and wavevector $\boldsymbol{k}(\omega_s)$, and one idler photon with frequency $\omega_i = \omega_p - \omega_s$ and wavevector $\boldsymbol{k}(\omega_i)$; the integration is carried out over the entire idler wave phase space $\mathcal{V}_i$. Note that we dropped here ordinary or extraordinary wave notation (index ν) for the sake of simplicity.

The transition matrix element with the use of Eq. (S6.4) is then:

$$< f\left|\hat{\mathcal{H}}_{int}\right|0> = \hbar\sqrt{\omega_s\omega_i}\frac{1}{V}c_{\boldsymbol{k}_s}c_{\boldsymbol{k}_i}\frac{1}{2}\sqrt{\frac{2P_p}{\varepsilon_0 c n_p A}}$$
$$\times\sum_{lmn}\bar{\bar{\chi}}^{(2)}_{lmn}u_l(\omega_p)u_m(\omega_s)u_n(\omega_i)\int_V d^3\boldsymbol{r}e^{i\Delta\boldsymbol{k}\boldsymbol{r}} \tag{S6.9}$$

where $\Delta\boldsymbol{k} = (\boldsymbol{k}_p - \boldsymbol{k}_{s\parallel} - \boldsymbol{k}_{i\parallel}) - (\boldsymbol{k}_{s\perp} + \boldsymbol{k}_{i\perp})$, $\boldsymbol{k}_p$ is the pump wavevector, $\boldsymbol{k}_{\xi\parallel}$ and $\boldsymbol{k}_{\xi\perp}$ are components of the signal (idler) wavevectors parallel and perpendicular to the pump one, respectively (not to mix with $\varepsilon_\perp$ and $\varepsilon_\parallel$ that are linked with axes of the uniaxial crystal, see Fig. 1(c) of the main text). In the limit of large crystal area, i.e., $A \to \infty$, the expression for the transition matrix element is transformed to:

$$< f|\hat{\mathcal{H}}_{int}|0 > = \hbar\sqrt{\omega_s\omega_i}\frac{4\pi^2}{V}c_{\boldsymbol{k}_s}c_{\boldsymbol{k}_i}\frac{1}{2}\sqrt{\frac{2P_p}{\varepsilon_0 c n_p A}}\times$$

$$\sum_{lmn}\bar{\bar{\chi}}^{(2)}_{lmn}u_l(\omega_p)u_m(\omega_s)u_n(\omega_i)\frac{1-e^{i\Delta k_\parallel L}}{i\Delta k_\parallel}\delta(\boldsymbol{k}_{s\perp}+\boldsymbol{k}_{i\perp}) \quad \text{(S6.10)}$$

where $\Delta k_\parallel = \left(\boldsymbol{k_p}-\boldsymbol{k}_{s\parallel}-\boldsymbol{k}_{i\parallel}\right)\frac{\boldsymbol{k}_p}{|\boldsymbol{k}_p|}$.

Let us go back to the rate equation, Eq. (S6.8). Using a standard Van Hove transformation $d^3\boldsymbol{k}_i = d^2\boldsymbol{s}_i\frac{d\omega}{\left|\nabla_{\boldsymbol{k}_i}\omega\right|}$ we arrive at [26]:

$$\mathcal{R}_s(\omega_s,k_s) = \frac{1}{\hbar^2}\int\limits_{\partial\mathcal{V}_i}\frac{V}{4\pi^2}\left|< f|\hat{\mathcal{H}}_{int}|0 >\right|^2\frac{1}{\left|v_g(\boldsymbol{k}_i)\right|}d^2\boldsymbol{s}_i \quad \text{(S6.11)}$$

where the integration is over the idler isofrequency surface $\partial\mathcal{V}_i$, for which $\boldsymbol{k}_i = \boldsymbol{k}_i(\omega_i=\omega_p-\omega_s)$, $d^2\boldsymbol{s}_i$ is the isofrequency surface element, and $v_g(\boldsymbol{k}_i) = \nabla_{\boldsymbol{k}_i}\omega_i$ is the idler group velocity.

However for our proceeding calculations, in which we consider pump propagation along some given direction, it is convenient to use $d^3\boldsymbol{k}_i = d^2\boldsymbol{k}_{i\perp}\frac{\partial\boldsymbol{k}_{i\parallel}}{\partial\omega}\,d\omega$ instead, where $\boldsymbol{k}_{i\perp}$ and $\boldsymbol{k}_{i\parallel}$ are the components of the idler wavevector perpendicular and parallel to the pump propagation direction, respectively. In this case the rate of signal photon emission is found as:

$$\mathcal{R}_s(\omega_s,\boldsymbol{k}_s) = \frac{1}{\hbar^2}\int\frac{V}{4\pi^2}\left|< f|\hat{\mathcal{H}}_{int}|0 >\right|^2\frac{\partial\boldsymbol{k}_{i\parallel}}{\partial\omega}d^2\boldsymbol{k}_{i\perp} \quad \text{(S6.12)}$$

here the integration is carried over an area in the idler wave phase space on a plane $\boldsymbol{k}_{i\parallel}=0$ bound by the isofrequency contour $\partial\mathcal{V}_i$. $\frac{\partial\boldsymbol{k}_{i\parallel}}{\partial\omega}$ has a meaning of the idler wave group velocity in the direction on the pump propagation.

So far in our quantization of the signal and idler fields, and in the study of their interactions, we have neglected dissipation, having considered real-valued material parameters at signal and idler photon frequencies, i.e., $\bar{\bar{\varepsilon}} \to \mathrm{Re}(\bar{\bar{\varepsilon}})$. Such an approach is justified when $\left|\frac{\mathrm{Im}(\bar{\bar{\varepsilon}})}{\mathrm{Re}(\bar{\bar{\varepsilon}})}\right| \ll 1$, as we have discussed earlier. We note that there is no such restriction on a pump wave, since it is treated classically (that is, we take into full consideration losses at the frequency of the pump). We treat signal and idler photon losses perturbatively. Specifically, we consider the interplay of probabilities of photon generation and subsequent absorption. In a lossless limit the probability of observing a signal photon at time t is $\mathcal{P}_s' = \mathcal{R}_s t$. In the presence of photon dissipation, this expression has to be modified. In particular, the probability of observing a signal photon emitted in the interval of time $\tau + d\tau$ at a later time t with accounting for the probability of subsequent photon absorption may be found as:

$$\delta\mathcal{P}_s(t,\tau) = \frac{d\mathcal{P}_s'(\tau)}{d\tau}d\tau e^{-\gamma(\boldsymbol{k}_s)(t-\tau)} \quad \text{(S6.13)}$$

where $\gamma(\boldsymbol{k}_s)$ corresponds to the signal photon dissipation rate that will be determined later. Here we assumed also independence of photon generation and absorption events. The overall probability of observing photon at time t is then $\mathcal{P}_s(t) = \int_0^t \delta\mathcal{P}_s(t,\tau)d\tau$. Hence the signal photon generation rate ($\mathcal{R}_s = \frac{d\mathcal{P}_s}{dt}$) with the account of dissipation is modified as:

$$\mathcal{R}_s \to \mathcal{R}_s e^{-\gamma(\boldsymbol{k}_s)t} \quad \text{(S6.14)}$$

here t has a meaning of interaction time, which we estimate as $t = \frac{L}{v_{g\parallel}(\boldsymbol{k}_s)}$, where L is the propagation length and $v_{g\parallel}(\boldsymbol{k}_s)$ is the group velocity of the generated signal photon with vector k_s at the frequency ω_s in the direction of pump propagation.

Next we estimate the downconverted signal photon power dP_s emitted per frequency interval $d\omega_s$ integrated over all possible emission angles, i.e., we calculate the emitted signal photon spectral power density:

$$\frac{dP_s}{d\omega_s} = \frac{V}{8\pi^3}\int\limits_{\mathcal{V}_s}\hbar\omega_s\mathcal{R}_s(\omega_s,\boldsymbol{k}_s)e^{-\gamma'(\boldsymbol{k}_s)L}\delta(\omega_s)d^3\boldsymbol{k}_s \quad \text{(S6.15)}$$

Here the integration is over entire signal photon phase space $\mathcal{V}_s$ and $\gamma_s'(\boldsymbol{k}_s) = \gamma(\boldsymbol{k}_s)/v_{g\parallel}(\boldsymbol{k}_s)$. Using $d^3\boldsymbol{k}_s = d^2\boldsymbol{k}_{s\perp}\frac{\partial\boldsymbol{k}_{s\parallel}}{\partial\omega}\,d\omega_s$ we find that:

$$\frac{dP_s}{d\omega_s} = \frac{\hbar\omega_s V}{8\pi^3}\int\frac{\partial\boldsymbol{k}_{s\parallel}}{\partial\omega}\mathcal{R}_s(\omega_s,\boldsymbol{k}_s)e^{-\gamma'(\boldsymbol{k}_s)L}d^2\boldsymbol{k}_{s\perp} \quad \text{(S6.16)}$$

Substituting the expressions for $\mathcal{R}(\omega_s,\boldsymbol{k}_s)$ and $< f|\hat{\mathcal{H}}_{int}|0 >$ into the Eq. (S6.16) we arrive to:

$$\frac{dP_s}{d\omega_s} = \frac{\hbar\omega_s^2\omega_i L^2}{2(2\pi)^3}\frac{P_p}{\varepsilon_0 c n_p}\int d^2\boldsymbol{k}_{s\perp}\frac{\partial\boldsymbol{k}_{s\parallel}}{\partial\omega}\frac{\partial\boldsymbol{k}_{i\parallel}}{\partial\omega}\,c_{\boldsymbol{k}s}^2c_{\boldsymbol{k}i}^2\times$$

$$\left|\sum_{lmn}\bar{\bar{\chi}}^{(2)}_{lmn}u_l(\omega_p)u_m(\omega_s)u_n(\omega_i)\right|^2\left|\frac{1-e^{i\Delta k_\parallel L}}{i\Delta k_\parallel L}\right|^2 e^{-\gamma'(\boldsymbol{k}_s)L} \quad \text{(S6.17)}$$

here it is assumed that transverse phase matching is satisfied (i.e., $\boldsymbol{k}_{i\perp} = -\boldsymbol{k}_{s\perp}$). We note that in the limit of isotropic, dispersionless and lossless system this expression simplifies to that given in Refs. [17, 17].

Finally making a transform $d\omega_s \to d\lambda_s$ we get:

$$\frac{dP_s}{d\lambda_s} = \frac{\hbar\pi c^3 L^2}{\lambda_s^4\lambda_i}\frac{P_p}{\varepsilon_0 n_p}\int d^2k_{s\perp}\frac{\partial k_{s\parallel}}{\partial\omega}\frac{\partial k_{i\parallel}}{\partial\omega}\,c_{ks}^2c_{ki}^2\times$$

$$\left|\sum_{lmn}\bar{\bar{\chi}}^{(2)}_{lmn}u_l(\omega_p)u_m(\omega_s)u_n(\omega_i)\right|^2\left|\frac{1-e^{i\Delta k_\parallel L}}{i\Delta k_\parallel L}\right|^2 e^{-\gamma'(k_s)L} \quad \text{(S6.18)}$$

This equation provides important insights into SPDC in a general uniaxial crystal. In particular, the photon emission rate depends on the interplay between the probabilities of SPDC photon generation, which grows linearly with interaction length L, and single photon absorption, which exponentially increases with distance, $e^{-\gamma'(k_s)L}$. In a nondegenerate case ($\omega_s \neq \omega_i$), emission at the signal wavelength may be tuned by controlling the idler wave dispersion. For instance, stronger signal photon generation is expected in the slow light regime at the idler frequency (when $v_{g\parallel}(k_i) \ll c$).

Next we estimate the decay rate $\gamma(\boldsymbol{k}_s)$ of generated signal photons. The mechanisms of single photon dissipation in metallic and nanophotonic structures are currently an active topic of research (see for instance Ref. [24]). Here we assume the most simple case of a photon coupled with a thermal reservoir (such a picture would correspond physically to an Ohmic-like dissipation in metallic systems within a Drude regime of dispersion). In this case standard quantum Langevin equations for photon annihilation (creation) operators may be derived:

$$\frac{d\hat{a}_{\boldsymbol{k}_s}}{dt} = -i\omega_s\hat{a}_{\boldsymbol{k}_s} - \frac{1}{2}\gamma_{QM}(\boldsymbol{k}_s)\hat{a}_{\boldsymbol{k}_s} + \hat{F}(t)e^{-i\omega_s t} \quad \text{(S6.19)}$$

where $\gamma_{QM}(\boldsymbol{k}_s)$ is the quantum mechanical decay rate that depends on the density of bath states and photon – reservoir coupling, and $\hat{F}(t)$ is the quantum noise operator.

For a reservoir in thermal equilibrium, the photon number expectation value corresponding to the classical electromagnetic field intensity may be found as:

$$\frac{d < \hat{a}_{\boldsymbol{k}_s}^+\hat{a}_{\boldsymbol{k}_s} >}{dt} = -\gamma_{QM}(\boldsymbol{k}_s) < \hat{a}_{\boldsymbol{k}_s}^+\hat{a}_{\boldsymbol{k}_s} > + \frac{\gamma_{QM}(\boldsymbol{k}_s)}{2}\frac{1}{e^{\frac{\hbar\omega_s}{kT}}-1} \quad \text{(S6.20)}$$

where the last term plays a role of a diffusion coefficient. At optical frequencies of interest $\hbar\omega_s \gg kT$ and therefore it may be neglected. Hence Eq. (S6.20) reduces to a well familiar classical equation for the field intensity dissipation, implying that $\gamma_{QM}(\boldsymbol{k}_s) \simeq \gamma(\boldsymbol{k}_s)$. The classical decay rate, $\gamma(\boldsymbol{k}_s)$, in the limit of $\left|\frac{\mathrm{Im}(\varepsilon)}{\mathrm{Re}(\varepsilon)}\right| \ll 1$ may be estimated from a Poynting theorem [22]:

$$\frac{d\hat{\mathcal{H}}_{lin}^s}{dt} = -\varepsilon_0\omega_s\int\limits_V d^3\boldsymbol{r}\sum_\nu \mathrm{Im}\left(\varepsilon_\nu(\omega_s)\right)\hat{E}_{s\nu}^2 \quad \text{(S6.21)}$$

here ν runs over the Cartesian coordinates. After some algebra we get:

$$\gamma(\boldsymbol{k}_s) = \omega_s c_{\boldsymbol{k}_s}^2\sum_\nu \mathrm{Im}\left(\varepsilon_\nu(\omega_s)\right)u_\nu^2 \quad \text{(S6.22)}$$

So far we have discussed fluorescence rate and spectral power density of the signal photon only. Emission of bi-photon states requires observing both signal and idler photons. By applying arguments similar to those preceding the derivation of Eq. (S6.14) we may estimate the coincidence rate as:

$$R_{coincidence} = \frac{\omega_s \omega_i L^2}{2(2\pi)^3} \frac{P_p}{\varepsilon_0 c n_p} \int d^2\boldsymbol{k}_{s\perp} \frac{\partial \boldsymbol{k}_{s\parallel}}{\partial \omega} \frac{\partial \boldsymbol{k}_{i\parallel}}{\partial \omega} c_{\boldsymbol{k}s}^2 c_{\boldsymbol{k}i}^2 \times \left| \sum_{lmn} \bar{\bar{\chi}}_{lmn}^{(2)} u_l(\omega_p) u_m(\omega_s) u_n(\omega_i) \right|^2 \left| \frac{1 - e^{i\Delta k_\parallel L}}{i\Delta k_\parallel L} \right|^2 \times \exp(-[\gamma'(\boldsymbol{k}_s) + \gamma'(\boldsymbol{k}_i)]L), \quad \text{(S6.23)}$$

here again it is assumed that transverse phase matching is satisfied (i.e., $\boldsymbol{k}_{i\perp} = -\boldsymbol{k}_{s\perp}$); $\gamma'(\boldsymbol{k}_i)$ is the idler photon decay rate, which can be found similarly to Eq. (S6.22).

Even in the case of both photons observed at the output of the system (i.e., not absorbed), one may question whether the entanglement between the emitted photons is preserved. For instance, entanglement may be altered by strong dispersion and interaction with the environment. Interestingly, number of recent experiments on plasmon quantum interference show that the entanglement is not affected by losses or dispersion [25-29].

It is noteworthy also that the experimental papers [25-29] corroborate our theoretical approach, indicating that eigenmode description and quantization introduced in our paper is valid even in a high loss high dispersion scenario.

Integration boundaries. Here we give explicit expressions for the integration boundaries in Eq. (S6.18).

For $\boldsymbol{z}$ directed prorogation of the pump wave, it is convenient to transform to an integral in polar coordinates, i.e., $d^2\boldsymbol{k}_\perp = k_\rho dk_\rho d\phi$. In this case the integration is as follows:

$$\int_0^{\frac{\omega}{c}\sqrt{\varepsilon_\parallel}} k_\rho dk_\rho \int_0^{2\pi} d\phi <> \quad for \quad \varepsilon_\perp > 0 \quad and \quad \varepsilon_\parallel > 0$$

$$\int_{\sqrt{\frac{\omega^2}{c^2}\varepsilon_\parallel - k_{z\max}\frac{\varepsilon_\parallel}{\varepsilon_\perp}}}^{\frac{\omega}{c}\sqrt{\varepsilon_\parallel}} k_\rho dk_\rho \int_0^{2\pi} d\phi <> \quad for \quad \varepsilon_\perp < 0 \quad and \quad \varepsilon_\parallel > 0$$

$$\int_0^{\sqrt{\frac{\omega^2}{c^2}\varepsilon_\parallel - k_{z\max}\frac{\varepsilon_\perp}{\varepsilon_\parallel}}} k_\rho dk_\rho \int_0^{2\pi} d\phi <> \quad for \quad \varepsilon_\perp > 0 \quad and \quad \varepsilon_\parallel < 0$$

For $\boldsymbol{x}$ direction of pump wave propagation we get:

$$\int_{-\frac{\omega}{c}\sqrt{\varepsilon_\parallel}}^{\frac{\omega}{c}\sqrt{\varepsilon_\parallel}} dk_y \int_{-\sqrt{\frac{\omega^2}{c^2}\varepsilon_\perp - k_y^2\frac{\varepsilon_\perp}{\varepsilon_\parallel}}}^{\sqrt{\frac{\omega^2}{c^2}\varepsilon_\perp - k_y^2\frac{\varepsilon_\perp}{\varepsilon_\parallel}}} dk_z <> \quad for \quad \varepsilon_\perp > 0 \quad and \quad \varepsilon_\parallel > 0$$

$$\int_{-k_{z\max}}^{k_{z\max}} dk_z \int_{-\sqrt{\frac{\omega^2}{c^2}\varepsilon_\parallel + k_z^2\frac{\varepsilon_\parallel}{|\varepsilon_\perp|}}}^{\sqrt{\frac{\omega^2}{c^2}\varepsilon_\parallel + k_z^2\frac{\varepsilon_\parallel}{|\varepsilon_\perp|}}} dk_y <> \quad for \quad \varepsilon_\parallel > 0 \quad and \quad \varepsilon_\perp < 0$$

$$2\int_{\frac{\omega}{c}\sqrt{\varepsilon_\perp}}^{k_{z\max}} dk_z \int_{-\sqrt{-\frac{\omega^2}{c^2}|\varepsilon_\parallel| + k_z^2\frac{|\varepsilon_\parallel|}{\varepsilon_\perp}}}^{\sqrt{-\frac{\omega^2}{c^2}|\varepsilon_\parallel| + k_z^2\frac{|\varepsilon_\parallel|}{\varepsilon_\perp}}} dk_y <> \quad for \quad \varepsilon_\perp > 0 \; and \; \varepsilon_\parallel > 0$$

where $k_{z\max} = \frac{2\pi}{\Lambda}$ is the maximum allowed wavelength in the system.

Note that at the integration boundaries $\frac{\partial k_\parallel}{\partial \omega}$ diverge. This issue can be resolved by transforms of the form $k = C\sin(\theta)$ or $k = C\cos(\theta)$, where C is a constant.

A note on quantization. In our analysis, we have used a common approach of quantizing an electric field $\boldsymbol{E}$ which is the solution of classical Maxwell equations. However, since $\boldsymbol{E}$ is not a canonical variable such an approach leads to a number of fundamental inconsistencies. Thus, Maxwell equations do not follow from the quantum mechanical formalism in a general case of an anisotropic medium. For instance, as was shown in Ref. [15, 16], $\frac{\partial \widehat{\boldsymbol{B}}}{\partial t} = \frac{i}{\hbar}\left[\widehat{\mathcal{H}}, \widehat{\boldsymbol{B}}\right] \neq -\nabla \times \widehat{\boldsymbol{E}}$ even in a linear dispersionless limit. This suggests that the quantization of the electromagnetic field has to be modified.

A proper quantum theory starts with identifying canonical variables and formulating a Hamiltonian of the system in terms of these variables. The magnetic vector potential $\boldsymbol{A}$ and scalar electric potential φ are typically chosen as such canonical variables. In an isotropic case quantization is easily formulated with the use of Coulomb gauge conditions, i.e., $\nabla \boldsymbol{A} = 0$ and $\varphi = 0$. However, for an anisotropic system $\nabla \boldsymbol{A} \neq 0$ since $\nabla \boldsymbol{E} \neq 0$ (this is actually one of the main reasons behind commonly employed direct quantization of the electric field in complex systems).

Instead, in the absence of external charges $\nabla \boldsymbol{D} = 0$ is always fulfilled [16]. This suggests the use of the electric vector potential $\boldsymbol{Z}$ ($\boldsymbol{D} = \nabla \times \boldsymbol{Z}$) as a canonical variable for electromagnetic field quantization. Importantly, $\boldsymbol{Z}$ satisfies Coulomb-like condition (i.e., $\nabla \boldsymbol{Z} = 0$ for any medium with $\mu = 1$). In the case of uniaxial crystals considered in this paper, this condition physically originates from the fact that ($\boldsymbol{D}$, $\boldsymbol{B}$) field is transverse inside the crystal (i.e., $\boldsymbol{D} \perp \boldsymbol{B} \perp \boldsymbol{k}$).

For the sake of completeness, we have used this formulation and developed a corresponding quantum mechanical model for spontaneous parametric down conversion in a general lossy dispersive anisotropic crystal. It is easy to show that the classical Hamiltonian of the system in CGS units can be expressed as:

$$\mathcal{H} = \frac{1}{2}\sum_\omega \int_V d^3\boldsymbol{r}\left[B^2 + \sum_l \frac{\partial \beta_l^{(1)}\omega}{\partial \omega} D_l^2\right] + \int_V d^3\boldsymbol{r} \sum_{lmn}\left[\beta_{lmn}^{(2)} D_l^*(\omega_p) D_m(\omega_s) D_n(\omega_i) + c.c.\right] \quad \text{(S6.24)}$$

where $\boldsymbol{D} = \nabla \times \boldsymbol{Z}$, $\boldsymbol{B} = \frac{1}{c}\frac{\partial \boldsymbol{Z}}{\partial t}$, $\bar{\bar{\beta}}^{(1)}$ and $\bar{\bar{\beta}}^{(2)}$ are first and second order electric permeabilities, $\bar{\bar{\beta}}^{(1)} = \bar{\bar{\varepsilon}}^{-1}$ and $\bar{\bar{\beta}}_l^{(2)} = -\sum_m \beta_{lm}^{(1)}(\omega_s)\, \bar{\bar{\chi}}_m^{(2)} \bar{\bar{\beta}}^{(1)}(\omega_i) \frac{1}{n_p^2}$.

Next quantizing the electric vector potential $\boldsymbol{Z}$ in a standard way and making derivations similar the ones shown above in this section, we get the expression for the signal photon power emission. We do not present such an analysis here.

In our calculations of the signal photon emission rate and power, we used both formalisms, i.e., the one based on electric field quantization and another one based on the electric vector potential quantization. Both of these theories give similar results.

S7. PROPOSED SYSTEMS FOR EXPERIMENTAL DEMONSTRATION

As discussed in the text, efficient luminescence is possible after ~100 nm of propagation, suggesting that a metallic grating carved into a nonlinear dielectric substrate with subwavelength spacing and straightforward-to-fabricate aspect ratio (~1/5) would serve as a simple-to-test system Fig. S6(a). Another experimental proposal is based on a recently demonstrated hyperbolic metasurface; loading it with a nonlinear medium may lead to a possibility for an on-chip bi-photon generation Fig. S6(b).

We note that the deposition of GaP and Lithium Niobate on top of metals might lead to polycrystalline structures with lower effective second

order susceptibilities. However, we believe that this issue may be circumvented by an inverse process. That is, one may nanopattern the structure in the single crystal material and then deposit required metals on top. The possibility of nanofabrication in bulk crystals has been widely discussed and demonstrated in literature [30-36].

An important issue is the outcoupling of emitted photons from hyperbolic metamaterials into the surrounding medium. We note the emission inside the hyperbolic media occurs only in a rather narrow range of preferential directions (see Fig. 4f in the main text). By identifying these preferential directions, it is possible to design a matching system between a surrounding medium and a hyperbolic metamaterial [37-41].

Hence, in Refs. [37,40] a grating geometry for an efficient outcoupling of emitted photons was demonstrated experimentally (up to 20x enhancement of photon extraction in these geometries was reported). In Ref. [38] a tapered hyperbolic metamaterial was studied. It was shown that a tapered geometry allows for an efficient and broadband light coupling in and out of hyperbolic media. The possibility of an efficient broadband light outcoupling mechanism is particularly relevant to our case, where we predict a broadband photon emission due to nonlinear downconversion. Importantly, in Ref. [38] estimates suggest about 50% of outcoupling efficiency for such a broadband system (with k vectors in the range of $\mathbf{0} \leq \boldsymbol{k} \leq \mathbf{10}\boldsymbol{k_0}$, i.e., similar to the ones predicted in our work, see Fig. 4f).

Given an experimentally feasible 50% of light outcoupling efficiency [42] (note that with a proper design >70% efficiency is possible [43]) we estimate that 50% of emitted signal and idler photons may be collected in the far field. Hence, the single photon fluorescence rates calculated in our paper will be reduced by a factor of 2. The coincidence rate may also be affected by loss of photons due to conversion of emitted high-k modes into the free-space. Particularly, the coincidence count will be reduced by a factor 0.25 as compared to the one "measured" inside the hyperbolic medium itself, Eq. (S6.23).

Finally, we note that with a growing interest to an on-chip integrated quantum optics, a need of outcoupling generated photons into an unbounded free space medium may be revisited. Hence, one may envision a dispersion engineered system (e.g., hyperbolic metamaterial) as a part of a more complex photonic integrated circuit, where the generated photons are then routed with the help of sub-diffraction optics components – plasmonic and high index dielectric [25-29,44,45].

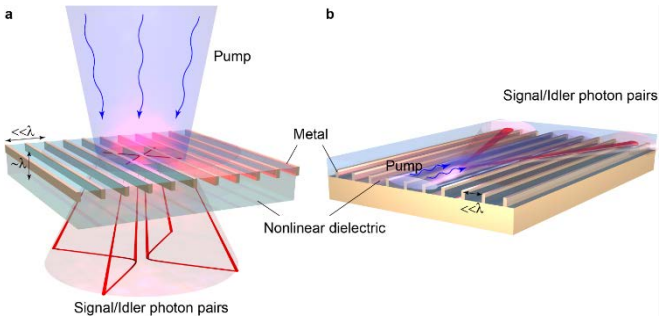

Fig. S6. Schematic illustration of configurations for possible experimental demonstration of the predicted mismatch-free Purcell enhancement of the nonlinear luminescence in hyperbolic metastructures. (a) a nonlinear metasurface with out-of-plane illumination. (b) an in-plane hyperbolic metasurface.

REFERENCES

1. P.B. Johnson and R.W. Christy, *Optical Constants of the Noble Metals,* Phys. Rev. B **6**, 4370 (1972).
2. Y. Liu and X. Zhang, *Metamaterials: a new frontier of science and technology,* Chem. Soc. Rev. **40**, 2494–2507 (2011).
3. N. Engheta and R.W. Ziolkowski, *Metamaterials: physics and engineering explorations* (John Wiley & Sons, 2006).
4. A. Poddubny, I. Iorsh, P. Belov, Y. Kivshar, *Hyperbolic metamaterials*, Nature Photon. **7**, 948-957 (2013).
5. A. Yariv and P. Yeh. Optical Waves in Crystals: Propagation and Control of Laser Radiation. (Wiley-Interscience, 2002).
6. D.E. Zelmon, D.L. Small, and D. Jundt, Infrared corrected Sellmeier Coefficients for Congruently Grown Lithium Niobate and 5 mol.% Magnesium Oxide-Doped Lithium Niobate, J. Opt. Soc. Am. B **14**, 3319-3322 (1997).
7. G.E. Jellison, Optical Functions of GaAs, GaP, and Ge Determined by Two-Channel Polarization Modulation Ellipsometry, Opt. Mat. **1**, 151-160 (1992).
8. M.O. Scully and M.S. Zubairy. *Quantum Optics.* 1st ed. (Cambridge University Press, 1997).
9. H.T. Dung, L. Knoll, and D.-G. Welsch, Three-Dimensional Quantization of the Electromagnetic Field in Dispersive and Absorbing Inhomogeneous Dielectrics, Phys. Rev. A **57**, 3931 (1998).
10. R. Matloob, R. Loudon, S.M. Barnett, and J. Jeffers, *Electromagnetic Field Quantization in Absorbing Dielectrics*, Phys. Rev. A **52**, 4823 (1995).
11. J.E. Sipe, *Photons in Dispersive Dielectrics,* J. Opt. A: Pure Appl. Opt. **11**, 114006 (2009).
12. N.A.R. Bhat and J.E. Sipe, Hamiltonian Treatment of the Electromagnetic Field in Dispersive and Absorptive Structured media, Phys. Rev. A **73**, 063808 (2006).
13. L.G. Suttorp and M. Wubs, Field Quantization in Inhomogeneous Absorptive Dielectrics, Phys. Rev. A **70**, 013816 (2004).
14. B. Huttner and S.M. Barnett, "*Quantization of the Electromagnetic Field in Dielectrics*, Phys. Rev. A **46**, 4306 (1992).
15. S.-T. Ho and P. Kumar, Quantum Optics in a Dielectric: Macroscopic Electromagnetic-Field and Medium Operators for a Linear Dispersive Lossy Medium - A Microscopic Derivation of the Operators and Their Commutation Relations, J. Opt. Soc. Am. B **10**, 1620 (1993).
16. M. Hillery and L.D. Mlodinow, *Quantization of Electrodynamics in Nonlinear Dielectric Media*, Phys. Rev. A **30**, 1860 (1984).
17. R.L. Byer and S.E. Harris, *Power and Bandwidth of Spontaneous Parametric Emission*, Phys. Rev. **168**, 1064 (1968).
18. M.H. Rubin, D.N. Klyshko, Y.H. Shih, and A.V. Sergienko, *Theory of Two-Photon Entanglement in Type-II Optical Parametric Down-Conversion,* Phys. Rev. A **50**, 5122 (1994).
19. L.D. Landau, L.P. Pitaevskii, and E.M. Lifshitz. Electrodynamics of Continuous Media, Second Edition: Volume 8 (Course of Theoretical Physics). 2nd ed. (Butterworth-Heinemann, 1984).
20. J.A. Armstrong, N. Bloembergen, J. Ducuing, and P. S. Pershan *Interactions between Light Waves in a Nonlinear Dielectric*, Phys. Rev. **127**, 1918 (1962).
21. P.S. Pershan, Nonlinear Optical Properties of Solids: Energy Considerations, Phys. Rev. **130**, 919 (1963).
22. R.W. Boyd. *Nonlinear Optics.* 3rd ed. (Academic Press, 2008).
23. N.W. Ashcroft and N.D. Mermin. *Solid State Physics.* (Cengage Learning, 1976).
24. A.M. Brown, R. Sundararaman, P. Narang, W. A. Goddard, and H. A. Atwater, *Nonradiative Plasmon Decay and Hot Carrier Dynamics: Effects of Phonons, Surfaces, and Geometry*, ACS Nano **10**, 957-966 (2016).
25. J.S. Fakonas et al., *Two-plasmon quantum interference*, Nat. Photon. **8**, 317–320 (2014).
26. E. Altewischer et al., *Plasmon-assisted transmission of entangled photons,* Nature **418**, 304–306 (2002).
27. R.W. Heeres et al., *Quantum interference in plasmonic circuits,* Nat. Nanotech. **8**, 719–722 (2013).

28. G. Di Martino et al., Observation of Quantum Interference in the Plasmonic Hong-Ou-Mandel Effect, Phys. Rev. Applied **1**, 034004 (2014).
29. J.S. Fakonas et al., *Path entanglement of surface plasmons*, New J. Phys. **17** 023002 (2015).
30. K. Rivoire et al., Multiply resonant photonic crystal nanocavities for nonlinear frequency conversion, Opt. Express **19**, 22198 (2011).
31. K. Rivoire et al., Gallium phosphide photonic crystal nanocavities in the visible, Applied Phys. Lett. **93**, 063103 (2008).
32. S. Liu et al., Resonantly enhanced second-harmonic generation using III-V semiconductor all-dielectric metasurfaces, arXiv (1608.02570)
33. M. Gloud et al., Large-scale GaP-on-diamond integrated photonics platform for NV center-based quantum information, J. Opt. Soc. Am. B **33**, B35 (2016).
34. H. Hartung et al., Ultra thin high index contrast photonic crystal slabs in lithium niobate, Opt. Materials **33**, 19 (2010).
35. F. Sulser et al., Photonic crystal structures in ion-sliced lithium niobate thin films, Opt. Express **17**, 20291 (2009).
36. H. Lu et al., Enhanced electro-optical lithium niobate photonic crystal wire waveguide on a smart-cut thin film, Opt. Express **20**, 2974 (2012).
37. T. Galfsky et al., Active hyperbolic metamaterials: enhanced spontaneous emission and light extraction, Optica **2**, 62 (2015).
38. P.R. West et al., Adiabatically Tapered Hyperbolic Metamaterials for Dispersion Control of High-k Waves, Nano Lett. **15**, 498 (2015).
39. L. Ferrari, et al., *Hyperbolic metamaterials and their applications,* Progress in Quantum Electronics **40**, 1 (2014).
40. K.V. Sreekanth et al., Large spontaneous emission rate enhancement in grating coupled hyperbolic metamaterials, Sci. Rep. **4**, 6340 (2014).
41. T.-H. Kao et al., Enhancement of light extraction based on nanowire hyperbolic metamaterials in a grating structure, Proceedings Volume 9883, Metamaterials X; 98830U (2016).
42. J. Lu et al., "Numerical optimization of a grating coupler for the efficient excitation of surface plasmons at an Ag–SiO2 interface," J. Opt. Soc. Am. B **24**, 2268 (2007).
43. W. Sun et al., "High-efficiency surface plasmon meta-couplers: concept and microwave-regime realizations," Light: Sci. & App. **5**, e16003 (2016).
44. F. Najafi et al., "On-chip detection of non-classical light by scalable integration of single-photon detectors," Nat. Comm. **6**, 5873 (2015).
45. J. Carolan et al., "Universal linear optics," Science 349, 6249 (2015).